Ocean Science

Impact of hydrographic data assimilation on the modelled Atlantic meridional overturning circulation

G. C. Smith[1,*]**, K. Haines**[1]**, T. Kanzow**[2,**]**, and S. Cunningham**[2]

[1]Environmental Systems Science Centre, University of Reading, Reading, UK
[2]National Oceanographic Centre, Southampton, UK
[*]now at: Environment Canada, Montreal, Canada
[**]now at: IFM-GEOMAR, University of Kiel, Kiel, Germany

Abstract. Here we make an initial step toward the development of an ocean assimilation system that can constrain the modelled Atlantic Meridional Overturning Circulation (AMOC) to support climate predictions. A detailed comparison is presented of 1° and 1/4° resolution global model simulations with and without sequential data assimilation, to the observations and transport estimates from the RAPID mooring array across 26.5° N in the Atlantic. Comparisons of modelled water properties with the observations from the merged RAPID boundary arrays demonstrate the ability of in situ data assimilation to accurately constrain the east-west density gradient between these mooring arrays. However, the presence of an unconstrained "western boundary wedge" between Abaco Island and the RAPID mooring site WB2 (16 km offshore) leads to the intensification of an erroneous southwards flow in this region when in situ data are assimilated. The result is an overly intense southward upper mid-ocean transport (0–1100 m) as compared to the estimates derived from the RAPID array.

Correction of upper layer zonal density gradients is found to compensate mostly for a weak subtropical gyre circulation in the free model run (i.e. with no assimilation). Despite the important changes to the density structure and transports in the upper layer imposed by the assimilation, very little change is found in the amplitude and sub-seasonal variability of the AMOC. This shows that assimilation of upper layer density information projects mainly on the gyre circulation with little effect on the AMOC at 26° N due to the absence of corrections to density gradients below 2000 m (the maximum depth of Argo).

The sensitivity to initial conditions was explored through two additional experiments using a climatological initial condition. These experiments showed that the weak bias in gyre intensity in the control simulation (without data assimilation) develops over a period of about 6 months, but does so independently from the overturning, with no change to the AMOC. However, differences in the properties and volume transport of North Atlantic Deep Water (NADW) persisted throughout the 3 year simulations resulting in a difference of 3 Sv in AMOC intensity. The persistence of these dense water anomalies and their influence on the AMOC is promising for the development of decadal forecasting capabilities. The results suggest that the deeper waters must be accurately reproduced in order to constrain the AMOC.

1 Introduction

The Atlantic Meridional Overturning Circulation (AMOC) involves a northward movement of warm upper waters accompanied by a southward movement of cold waters at depth. There is evidence that natural variations in the AMOC can affect climate over decadal timescales (e.g. Knight et al, 2005). Furthermore, forecasts presented by the Intergovernmental Panel on Climate Change (Meehl et al., 2007) suggest that the AMOC may slow down in response to greenhouse gas forcing, reducing the northward transport of heat by the Atlantic Ocean, and leading to a cooling of northern Europe that could offset anthropogenic warming. Evidence from paleoclimate records suggests that the AMOC can undergo very rapid transitions, such as a total shutdown in little more than a decade (Jansen et al., 2007). It is possible that increasing levels of greenhouse gases could trigger such a rapid change,

with potentially serious consequences for societies in Europe and other regions surrounding the Atlantic basin.

In the face of such risks, there is an obvious need for better, more quantitative, forecasts of the future behaviour of the AMOC: an AMOC prediction system could potentially provide a valuable early warning of imminent climate change. There is evidence that changes in the AMOC, and related climate impacts, may be predictable on decadal timescales (Griffies and Bryan, 1997; Collins et al., 2003, 2006; Dunstone and Smith, 2010). This evidence is based on studies that assume near perfect knowledge of the initial ocean state and a perfect model. An important research question is whether potential predictability translates into actual prediction skill, when forecasts are initialized using real ocean observations. This is a much harder challenge because of limited observational data and problems arising from model bias. Nevertheless, recent studies (Smith et al., 2007; Keenlyside et al., 2008) have shown evidence that ocean initialization does lead to enhanced skill in decadal forecasts of global mean surface temperature, relative to reference forecasts that use changing radiative forcing but are not initialized. These results are encouraging for the prospects of building a decadal forecasting capability.

However uncertainty exists regarding the state of the ocean, which leads to uncertainty in the ocean initial conditions required for climate forecasts, resulting in larger forecast errors. The synthesis of ocean models and observations through data assimilation has been shown to constrain the ocean state estimate, which in turn leads to improved forecasting skill (Vidard et al., 2007). Corrections to upper layer temperature and salinity through assimilation should lead to improved density gradients and hence geostrophic currents and transports. Indeed, assimilation has been shown to improve the representation of the AMOC mean intensity and temporal variability (Balmaseda et al., 2007), as well as the agreement with published estimates from five transatlantic sections (Bryden et al., 2005). However the CLIVAR-GSOP (Global Synthesis and Observations Panel) intercomparison of the AMOC in various reanalysis products revealed large disagreements (Köhl, 2006). These differences were attributed to a combination of factors including variations in: ocean model configurations and resolutions, assimilation methods, and observational datasets used. An additional major source of uncertainty is related to the paucity of historical ocean observations that may only impose a weak constraint on the system.

Further advances in predicting the AMOC and its impacts on climate require better climate models, better observations of the ocean state, and improvements to ocean syntheses. In this context, the first direct continuous measurements of the AMOC, as provided by the RAPID array (Cunningham et al., 2007), are of particular importance. In the first place, these new measurements can be used to evaluate existing analyses and forecasts, offering an unprecedented opportunity to assess the representation of the AMOC and related quantities.

For example, Baehr et al. (2009) use the RAPID array data to evaluate AMOC variability in simulations from a coupled climate model (ECHAM5/MPI-OM) and the ECCO-GODAE state estimate. In the second place, the data can be assimilated to generate improved estimates of initial conditions for coupled models and perhaps improvements in forecast skill. In this paper we focus on the first of these steps, using a global ocean GCM at two different resolutions (1° and 1/4°) to quantify the AMOC in these models and assess the impact of sequential hydrographic data assimilation. The syntheses presented here assimilate all available in situ hydrography (e.g. Argo, XBT) apart from data from the RAPID array which is used for an independent evaluation. The assimilation of in situ temperature and salinity observations allows for corrections to the hydrography in mid-basin down to a maximum depth of 2000 m. The RAPID array is used to test the model circulations against these results and allows us to assess what additional information could be gained from assimilating RAPID array data. The current study builds on the work of Baehr et al. (2009) by showing how the modelled AMOC is affected by sequential data assimilation (where the model density gradients are modified directly through assimilation increments) as well as demonstrating the influence of initial conditions on the modelled AMOC.

Section 2 introduces the model, the data available for assimilation and the assimilation method used. Section 3 describes the RAPID array data and discusses how the RAPID transports are calculated, and also presents different ways of comparing these data with the model results. Section 4 presents the results of a number of different assimilation experiments designed to understand what aspects of the AMOC can be recovered from the assimilation experiments. Section 5 looks at the effect of initial conditions on the modelled AMOC. Finally, Sect. 6 provides a discussion and conclusions on how the RAPID array data can best be used with models.

2　Description of model and experiments

2.1　Model description

The numerical model used here is the NEMO coupled ice-ocean model (Madec, 2008) version 2.3, based on the OPA9 ocean model (Madec et al., 1998) and the LIM2.0 sea ice model (Louvain sea Ice Model: Fichefet and Maqueda, 1997; Goosse and Fichefet, 1999). The ocean model is a primitive equation z-level model making use of the hydrostatic and Boussinesq approximations. The model employs a free surface (Roullet and Madec, 2000) with partial cell topography (Adcroft et al., 1997). The version used here has a tri-polar "ORCA" grid and 46 levels in the vertical, with thicknesses ranging from 6 m at the surface to 250 m at the ocean floor.

Two different model configurations have been used. The first has a global 1° resolution with a tropical refinement

to 1/3° (ORCA1). The second is a global eddy-permitting model at 1/4° resolution (ORCA025). Both configurations have been developed through the DRAKKAR Consortium (Barnier et al., 2007) and use model parameter settings as defined in Barnier et al. (2008) and Penduff et al. (2009). Both configurations employ an energy-enstrophy conserving momentum advection scheme (Barnier et al., 2008) and a Laplacian diffusion. Horizontal viscosity is parameterized with a biharmonic operator in ORCA025, and a Laplacian in ORCA1. Additionally, ORCA1 makes use of the Gent and McWilliams (1990) mixing parameterization. Vertical eddy diffusivity and viscosity coefficients are computed from a level 1.5 turbulent closure scheme using a prognostic equation for the turbulent kinetic energy (Blanke and Delecluse, 1993). Specific technical details regarding the implementation of this scheme can be found in Madec (2008). Juza et al. (2010) provide a comparison of the mixed layer depths produced using this turbulent closure scheme in the DRAKKAR model configurations. In addition, a detailed evaluation and comparison of these model configurations with satellite sea surface height observations is given by Penduff et al. (2009).

Surface atmospheric forcing for the model is obtained from the DRAKKAR Forcing Set 3 (DFS3; Brodeau et al., 2009). DFS3 is a hybrid dataset making use of temperature, humidity and winds from the ERA40 atmospheric reanalysis (1958–2001) and the ECWMF operational analyses thereafter (2001–2005). Short and long wave radiative fluxes are obtained from the Common Ocean Reference Experiment (CORE) dataset (Large and Yeager, 2004), which are derived from the International Satellite Cloud Climatology Project. Precipitation and snow fields have also been taken from CORE and have been subsequently modified to provide a more balanced global freshwater budget.

2.2 Assimilation scheme

Here, we use the $S(T)$ assimilation scheme (Smith and Haines, 2009), which is a sequential scheme for hydrographic data based on an Optimal Interpolation approach. Temperature profiles (T) are assimilated along with a salinity balancing increment as advocated by Troccoli and Haines (1999). Salinity profiles (S) are then assimilated along isotherms (i.e. $S(T)$) as advocated by Haines et al. (2006). By evaluating model errors as $S(T)$ rather than on depth levels $S(z)$, the large dynamical variability present in $S(z)$ is removed (i.e. heaving of water up and down), allowing a more accurate assessment of water mass errors. Second, $S(T)$ increments can be spread along isotherms so that corrections to a particular water mass do not influence adjacent water masses, which may have uncorrelated errors.

Model-data differences are evaluated at the closest model time step, and assimilation increments are calculated every 5 days (73 cycles per year). Increments are then introduced into the model evenly over the following day (known as In-

cremental Analysis Updating, see Bloom et al., 1996). Smith and Haines (2009) give more details of the assimilation and report on experiments all performed with the 1° resolution ORCA1 model looking at the impact of Argo data in a 3 year reanalysis of the period 2002–2004. The only change to the assimilation system here from that presented in Smith and Haines (2009) is the addition of balancing increments for sea surface height and geostrophic velocity to reduce variability induced by the model adjustments.

In situ temperature and salinity observations are obtained from the UK MetOffice quality controlled EN-ACT/ENSEMBLES dataset (Ingleby and Huddleston, 2007). This dataset is largely composed of observations from the World Ocean Database 2005 (Boyer et al., 2006) and supplemented by data from the GTSPP (Global Temperature and Salinity Profile Program) and Argo autonomous profiling floats (Gould, 2005). As such, the dataset includes all available hydrographic observations, including those from shipboard Expendable Bathythermographs (XBTs) and Conductivity-Temperature-Depth (CTD) measurements, as well as observations from mooring arrays (such as TAO and PIRATA). The operational quality control system used for the UK MetOffice FOAM assimilation products (Martin et al., 2007) is used to perform a number of consistency checks on the data. These include buddy checks, track checking, testing for density inversions and thinning of the data. A detailed description of the data included and the quality control processing is presented in Ingleby and Huddleston (2007). The version of the dataset used here (EN3_v1c) differs from previous versions of the dataset (e.g. EN2, EN3_v1a and EN3_v1b) in several ways (see www.hadobs.com for details); in particular the Argo data from SOLO/FSI floats have been omitted due to errors in the reported pressure levels.

2.3 Experiment design

The simulations here focus on the period from January 2002 to April 2005, allowing comparison with the first complete year of the RAPID array results (deployed in April 2004). Initial conditions for most experiments with both the 1° and 1/4° resolution models were taken from multi-decadal control simulations. Control simulations begin in 1958 following a 10-year spin up from the World Ocean Atlas 2001 (WOA; Conkright et al., 2002) water mass properties, and employ surface forcing from DFS3 (Brodeau et al., 2009). The 1/4° control run is designated CTL025 and was performed by the DRAKKAR consortium (Barnier et al., 2007) as run ORCA025-G70, while the 1° control run we designate CTL, which has been referred to previously as ORCA1-R70 (Barnier et al., 2007; Penduff et al., 2009).

A description of experiments and their motivation is set out below (and summarized in Table 1), with all experiments referring to the 1° resolution model except the last pair;

- The overall effect of assimilation in correcting errors was tested by starting assimilation in January 2002

Table 1. Experiment details. Here, WOA refers to the World Ocean Atlas 2001 (Conkright et al., 2002).

Experiment	Initial Condition	Period	Assimilation	Comment
CTL	Clim: WOA	1958–2005	No	Multi-decadal control run
SYN	CTL, 31 Dec 2001	2002–2005	Yes	Assimilation from spun-up I. C.
CTL-IC	Clim: WOA	2002–2005	No	Short control run
SYN-IC	Clim: WOA	2002–2005	Yes	Assimilation from climatology I. C.
CTL025	Clim: WOA	1958–2005	No	Multi-decadal control run
SYN025	CTL025	1987–2005	Yes	Assimilation from spun-up I. C.

(SYN) from the control run (CTL) conditions. Section 4 shows the improvements to the modelled temperature and salinity fields in the Atlantic provided by assimilation and the effect on transports at 26° N as compared to estimates from the first year of the RAPID array (March 2004–April 2005). The initial response and adjustment of the AMOC is discussed in Sect. 5.

– CTL contains significant errors associated with drifts and biases developed over the 44 years of simulation prior to 2002. To investigate the influence of starting from better water masses two experiments (with and without assimilation) are made starting in January 2002 with WOA climatology initial conditions and are presented in Sect. 5 (SYN-IC and CTL-IC respectively).

– Finally, the impact of resolution is studied using the 1/4° resolution control (CTL025) with a 1/4° assimilation experiment initialized from the control in January 1987 (SYN025; referred to previously as UR025.1). A comparison with the first year of RAPID array transport estimates (March 2004–April 2005) shows similar results to those of the 1° resolution model and is included in the supplementary material section.

3 Description of RAPID array and transport calculations

3.1 The RAPID monitoring array

The RAPID monitoring array was deployed across 26.5° N in the Atlantic ocean starting in April 2004 and is presently funded until at least 2013. The array consists of moorings on the western boundary of the Atlantic, on either side of the mid-Atlantic ridge, and on the eastern boundary slope (Fig. S1). The moorings provide continuous measurements of the hydrography in these areas and are supplemented by current meter measurements at the western boundary (see Kanzow et al., 2008 for a detailed description of the mooring array and instrumentation). The transports calculated from this array can be combined with the cable data monitoring of the Florida Current transport between Florida and the Bahamas (Baringer and Larson, 2001), and estimates of Ekman transport from wind data, to give a total AMOC at 26.5° N in the Atlantic.

Cunningham et al. (2007) (C07 hereafter) and Kanzow et al. (2007) describe how meridional transports and the AMOC can be calculated from the array and other data. There are a number of assumptions required to which the resulting transport estimates may be sensitive. In particular, the calculation of the barotropic circulation components, which cannot be monitored directly by density measurements, and the calculation of transports very close to the western boundary, make comparisons with modelled results, even for the higher resolution 1/4° model, difficult. We therefore need to review the key measurements and the calculations made from them to put the model results in context.

3.2 AMOC calculation from the model

Here we describe the methods used to calculate the model equivalent of the RAPID array observations and transport estimates shown in C07. In both model resolutions the continental slope along the western boundary at 26.5° N is represented by a vertical wall adjacent to several shallow grid points representing the Blake Plateau and Bahamas, with a well-defined Florida Strait to the west (Fig. 1).

The "mid-ocean transport" in C07 is calculated from zonal density gradients obtained by merging the temperature and salinity data from separate moorings into single profiles for the eastern and western boundaries. The mid-Atlantic ridge data is not used. At the western boundary, the merged density profile contains data mainly from a tall mooring array, referred to as WB2, located roughly 16 km offshore (Fig. S2). Geostrophic transports obtained from these merged density profiles are combined with current meter transports covering a "western boundary wedge" (WBW) along the continental slope to give the mid-ocean transport.

To simulate this configuration, model currents from the first shallow grid point on the shelf directly adjacent to the continental slope and those westward to Abaco Island (Bahamas) are used to represent the WBW observed by current
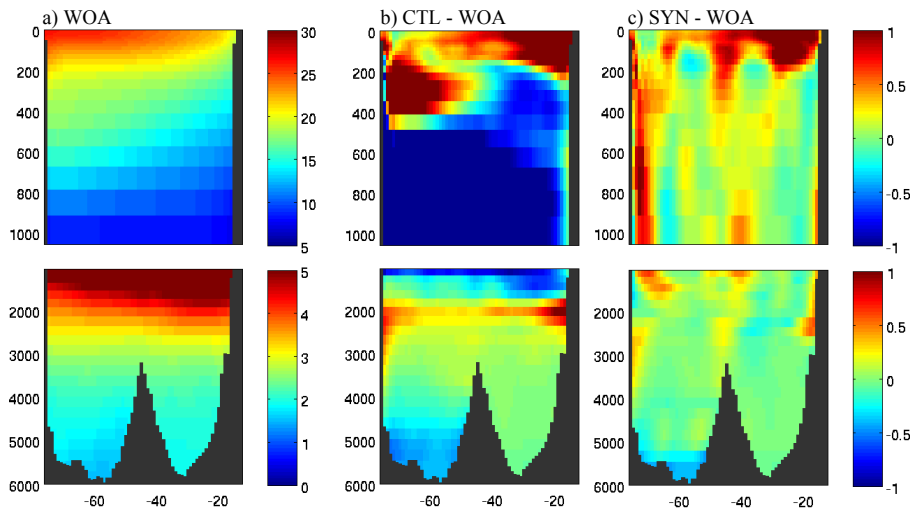
Fig. 1. Annual-mean cross-section of temperature at 26.5° N for the World Ocean Atlas (WOA) 2001 climatology **(a)** and the annual-mean 2004 anomalies from WOA for CTL **(b)** and SYN **(c)**. Note the large cold anomaly in CTL between 400–1000 m, due to a weak subtropical gyre circulation, which is corrected in SYN.

meters (Fig. S2). The hydrography in the first deep model column adjacent to the western continental slope is then compared to the RAPID array's merged western boundary profile. The eastern-most model grid point at each depth is used to compare to the RAPID array's merged eastern profile. These boundary profile comparisons are examined in Fig. 2 (temperature and salinity) and Fig. 3 (east and west boundary densities, ρ_E and ρ_W respectively). The separate contributions of the WBW and offshore transports are examined in Fig. 4.

Here we are interested in the change in meridional transports resulting from improvements to the cross-basin density gradients due to assimilation in the different model runs. Ignoring the mid-Atlantic ridge, the geostrophic meridional transport, V_{TW}, can be obtained by integrating the thermal wind equation upwards from the deepest observed depth, D, as

$$V_{\mathrm{TW}}(z) = -\frac{g}{\rho_0 f} \int_D^z \left(\frac{\rho_E(z) - \rho_W(z)}{L_x(z)} \right) dz \qquad (1)$$

where L_x is the distance between the western profile and the easternmost grid point, g is the gravitational acceleration, f the Coriolis parameter and ρ_0 is a reference density. Figure 3 shows the transports obtained using Eq. (1) along with an assumption of no motion at the deepest observed level, i.e. $V_{\mathrm{TW}}(D){=}0$. Due to the omission of the deep flow of Antarctic bottom water, and therefore the level of no motion applied in this calculation, these transports do not represent the total meridional flow and differ from the transports of C07 (their Fig. 1). However a comparison of the water properties at the east and west boundaries in the model to those observed, will help us understand the extent to which assim-
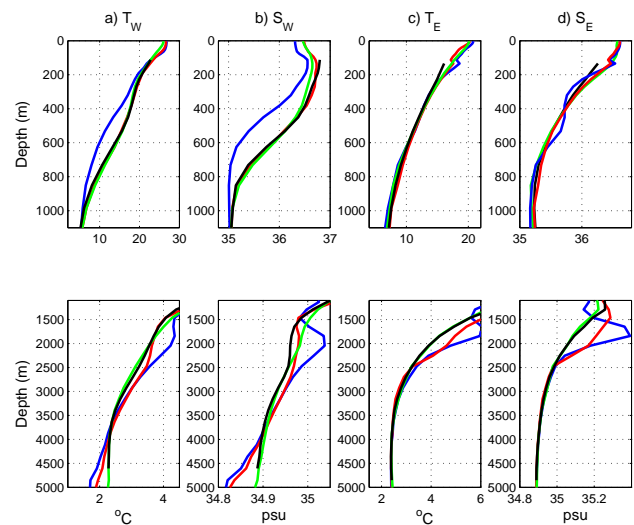
Fig. 2. Comparison of temperature (T) and salinity (S) at the western **(a, b)** and eastern **(c, d)** boundaries for experiments CTL (blue line) and SYN (red line) with merged observations from the RAPID boundary arrays (black line) and the World Ocean Atlas 2001 climatology (WOA; green line). Note the difference in scales for the upper (0–1100 m) and lower panels (1100–5000 m).

ilation constrains the zonal density gradient contribution to the mid-ocean transports.

In addition we examine the three AMOC components defined by C07: the wind-induced surface Ekman flow, the Florida Current transport and the mid-ocean transport. For this purpose, we interpret the timeseries from C07 as "best estimates" of the various components (and AMOC), and thus compare to exact model values of these transports rather than
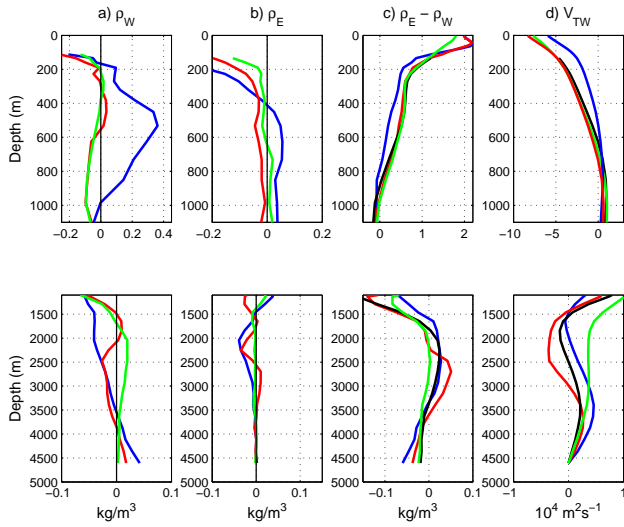
Fig. 3. Comparison with merged RAPID array density measurements at the western **(a)** and eastern **(b)** boundaries. The difference between CTL and SYN simulations and RAPID are shown as blue and red lines respectively, and the difference between the World Ocean Atlas (WOA) 2001 climatology and RAPID as a green line. Also shown are the east-west density differences **(c)** and the meridional transports per unit depth **(d)** for CTL, SYN and WOA compared to RAPID (black line). The meridional transports are estimated by integrating the thermal wind equation (Eq. 1) and assuming a level of no motion at the deepest observed depth. Note the difference in scales for the upper (0–1100 m) and lower panels (1100–5000 m).

estimates using the geostrophic methodology employed by C07.[1]

The Ekman volume transport, T_{Ek}, is obtained by zonal integral of the wind stress at 26.5° N, $\tau(x)$, as

$$T_{Ek} = -\frac{1}{\rho_0 f} \int_0^{L_B} \tau(x)dx \qquad (2)$$

where L_B is the full basin width from the Bahamas to Morocco. As both model configurations have a well-defined Florida Strait bounded by the Bahama Islands and Florida, the volume transport in the Florida Current can be obtained by simply integrating the meridional velocities vertically and zonally across the strait. Finally, the mid-ocean transport is calculated here as the vertical and zonal integral of the meridional volume flux from the Bahamas to the eastern boundary, minus the Ekman volume transport.

The mid-ocean transport can be further decomposed in the vertical into transports in the thermocline recirculation

---

[1]This may result in a difference of a few Sv (Baehr et al., 2009), and indeed we do obtain a slightly more favourable comparison with C07 when geostrophic transports are used in place of full velocities (not shown).
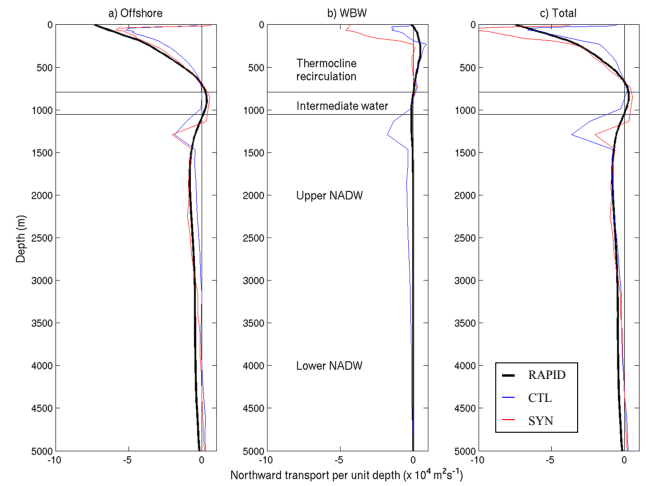
Fig. 4. Vertical profile of annual-mean northward transport per unit depth. Transports are shown for **(a)** the offshore component (eastward of RAPID mooring WB2), **(b)** the western boundary wedge (WBW; Abaco Island to WB2) and **(c)** the total meridional transport excluding the Florida Current (i.e. the sum of panel a and panel b). The annual mean is taken over the period of the first year of the RAPID array deployment (April 2004–April 2005). The CTL and SYN simulations are shown as blue and red lines respectively. Estimates from the RAPID array (C07) are shown as thick black lines. Model transports are calculated using full model velocities.

(0–800 m), the intermediate layer (800–1100 m), the upper North Atlantic Deep Water (NADW; 1100–3000 m) and the lower NADW (3000–4730 m). Note that in this vertical decomposition only the thermocline layer transport (0–800 m) has the Ekman transport subtracted. These depth ranges were selected for comparison with the estimates of C07. The lower depth limit for the lower NADW corresponds to the deepest observed zonal density gradient from the RAPID array and omits a small northward transport of Antarctic Bottom Water.

Note that all calculations presented here have been repeated using model grid points slightly to the north and south of 26.5° N, and no appreciable differences were found. In addition, several experiments were performed with the 1° resolution model configuration to adjust the depth of the sills and islands around the Bahamas to more accurately reflect the actual bathymetry. While this changes some details of the local circulation, the meridional transports around 26° N were not substantially affected.

4 Evaluation of model experiments at 26.5° N

We first present the general hydrography of the control and assimilation experiments (Sect. 4.1). Section 4.2 compares the model experiments to RAPID boundary array observations to assess the impact of hydrographic assimilation on mean geostrophically-derived volume transports. Section 4.3 makes comparisons using the full meridional velocities from

the model. Section 4.4 and 4.5 look at the time evolution of the "mid-oceanic transports" and the AMOC components respectively, showing the main result found here, that the gyre intensity can be greatly improved through assimilation and yet with little impact on the AMOC itself. The timescales of these adjustments and the impact of initial conditions are explored in Sect. 5.

4.1 Basic evaluation of model experiments

A detailed evaluation of the $S(T)$ assimilation method and the impact of assimilation on the modelled temperature and salinity across the various global basins is provided by Smith and Haines (2009) and thus only a brief description is provided here. Assimilation is found to eliminate many biases present in the free-model run and leads to a significant improvement in the agreement with independent in situ hydrographic observations. Gemmell et al. (2008, 2009) show that use of the $S(T)$ assimilation method leads to a better representation of certain mode waters and water mass properties. In addition, they show that this assimilation method provides an ocean state estimate which is in better agreement with in situ temperature and salinity observations than many other synthesis products. The improved agreement with observations is due in part to the more physical treatment of the data by the $S(T)$ assimilation method, but also to the relative errors applied to the model and observations. As such, the results presented here should be considered as being strongly constrained to data.

To illustrate the spatial structure of changes imposed by the assimilation, we show the 2004 annual-mean Atlantic temperature cross-section at 26.5° N between Abaco Island (Bahamas) and Morocco for CTL and SYN as anomalies from the World Ocean Atlas 2001 climatology (Conkright et al., 2002) in Fig. 1. The CTL simulation exhibits a large-scale cold bias between 400–1000 m, associated with a weak subtropical gyre circulation. Smith and Haines (2009) demonstrate that this bias is mainly of a dynamical origin, and may be corrected through a vertical heave of water masses without requiring a modification to water mass properties (i.e. $S(T)$). Figure 1 shows clearly that this bias has been corrected by assimilation and is no longer present in SYN. In addition, a warm bias above 400 m can be seen in the CTL simulation due to errors in the Gulf Stream separation, which have been improved in SYN.

Since the deepest observations in this region are from Argo, which only provide observations over the upper 2000 m, the direct influence of temperature and salinity assimilation does not penetrate below this depth. As such, model biases below 2000 m present in CTL can only be affected indirectly; for example, by improved transports or the advection of corrected waters below 2000 m. In particular, a cold anomaly found in CTL below 4000 m on the western side of the mid-Atlantic ridge can be seen to persist in SYN. As CTL shows a warm, saline bias below 1000 m in the sub-

polar gyre (not shown), this anomaly is likely associated with insufficient entrainment of dense NADW from the subpolar gyre, which results in an overly large penetration of Antarctic Bottom Water at depth (AABW) at 26° N. As there are no observations assimilated below 2000 m, the assimilation is unable to directly correct this model error locally. While some upstream correction may be possible (e.g. North of Denmark Strait or in the Labrador Sea), the SYN experiment is not long enough to see this effect. We show in Sect. 4.4 that the presence of this error at depth has an important impact on the modelled volume transports at 26.5° N and results in a weak AMOC.

4.2 Boundary profiles

Figures 2 and 3 show the mean model properties at the western and eastern boundaries compared against the WOA climatology and the first-year RAPID array merged boundary profiles (averaged over April 2004–March 05 corresponding to C07). Leaving aside the upper 300 m, the cold, fresh anomaly between 300–1000 m associated with the weak gyre circulation in CTL is seen at the western boundary (Fig. 2a,b) to represent errors of as much as 5 °C and 1 psu. These errors result in a positive density bias of nearly 0.3 kg/m³ (Fig. 3a). The assimilation provides a correction to both temperature and salinity errors bringing experiment SYN into excellent agreement with both climatology and the RAPID array measurements (Fig. 2a, b) and reduces the density error to less than 0.1 kg/m³. The correction of the western boundary densities also leads to a significant increase in the zonal density gradient in the upper layer (Fig. 3c), intensifying the subtropical gyre.

Between 1500–3500 m (Fig. 2, lower panels), there is a warm, saline error associated with weak NADW formation that can be seen on both sides of the basin in CTL, and which is only partially corrected in SYN. This bias in the NADW properties results in a negative density anomaly of up to 0.05 kg/m³ (Fig. 3a). As there are no observations assimilated below 2000 m, there is little improvement of this error in SYN over CTL below 2000 m. In addition, a cold, fresh anomaly in CTL below 4000 m is similarly unaffected in SYN due to a lack of observations. Note that, in general, the WOA climatology and RAPID provide similar values at the western and eastern boundaries showing that the errors present in CTL are due to model bias. A notable exception is the positive density anomaly on the western boundary (Fig. 3a) below 2000 m due likely to spatial smoothing in the WOA fields.

The implication of the changes between CTL and SYN in the zonal density gradient for offshore geostrophic transports (i.e. neglecting Florida Current and western boundary wedge contributions), can be inferred by application of the thermal wind equation (Eq. 1) with a level of no motion applied at the maximum observed depth of the RAPID Array. The resulting transport estimates are shown in Fig. 3d. One can see that the

Table 2. Annual-mean meridional transports over the upper 800 m at 26.5° N (April 04–March 2005). Transports are split into two components, an offshore component from RAPID mooring WB2 (roughly 16 km offshore) eastward to Morocco, and a western boundary wedge (WBW) between Abaco Island (Bahamas) and WB2. For the model, WB2 is assumed to be the first deep grid point (>3000 m) next to the continental shelf. Measurements from the RAPID array are obtained using moored current meters (see C07 for details).

Transport	Offshore	WBW	Total
CTL	−9.8 Sv	−4.8 Sv	−14.6 Sv
SYN	−19.0 Sv	−6.7 Sv	−25.7 Sv
RAPID	−19.1 Sv	+2.2 Sv	−16.9 Sv

Table 3. Annual-mean meridional layer transports at 26.5° N (April 2004–March 2005). Transports are split into four depth ranges, corresponding to the thermocline recirculation (0–800 m), the intermediate water (800–1100 m), the upper NADW (1100–3000 m) and the lower NADW (below 3000 m). Model values are calculated by integrating the meridional velocities across the full basin (from Abaco to Morocco). The RAPID values are quoted from C07.

Transport	0–800 m	800–1100 m	1100–3000 m	Below 3000 m
CTL	−14.6 Sv	−0.3 Sv	−12.7 Sv	−1.6 Sv
SYN	−25.7 Sv	+1.2 Sv	−13.4 Sv	−1.8 Sv
RAPID (C07)	−16.9 Sv	+0.7 Sv	−10.7 Sv	−7.8 Sv

improvements at mid-depth result in a stronger southward flow for SYN over the upper 1000 m, correcting the weak flow in CTL and providing an excellent agreement with the equivalent RAPID array estimates.

4.3 Vertical profile of meridional transports

The actual meridional transport between Abaco Island (the Bahamas) and Morocco depends on the full zonal pressure gradient evaluated on the two boundaries, which can differ from that determined using the difference between the merged boundary arrays, because the western array (mostly mooring WB2) is roughly 16 km offshore (Fig. S2). Thus, the analysis in the previous section omits a small "western boundary wedge" (WBW) between RAPID mooring WB2 and Abaco Island. The transport through this WBW is measured by the RAPID array using a series of moorings equipped with current meters. To more carefully assess the impact of assimilation on the mid-ocean transport, we separate the contributions from the WBW and the rest of the basin (i.e. from WB2 to the eastern boundary, or in the model from the continental shelf break to the eastern boundary) and compare transport estimates from the RAPID array with the full model velocities (Fig. 4).

The mean offshore transports (i.e. the mid-ocean transport excluding the WBW) obtained using the full model velocities (Fig. 4a) confirm the main features noted above from the geostrophic estimates (Fig. 3d). In the offshore thermocline recirculation (0–800 m), CTL has a notably weak mean southwards flow (−9.8 Sv), whereas the assimilation has intensified the gyre circulation in SYN (−19.0 Sv), bringing it in close agreement with the RAPID estimates of C07 (−19.1 Sv).

However, the mean transport in the WBW (Fig. 4b) in SYN (−6.7 Sv) is poorly constrained[2], and leads to the in-

tensification of an erroneous southwards flow[3] in the upper 300 m present in CTL (−4.8 Sv), increasing the discrepancy with the current meter measurements from RAPID (+2.2 Sv) (Table 2). The increased transport in the WBW in SYN is related to an equivalent increase in the Florida Current transport (discussed later in Sect. 4.5). As a result of this overly strong WBW transport, the total mid-ocean transport (Fig. 4c) in the thermocline recirculation in SYN is too large (−25.7 Sv). Whereas in CTL, the errors in the offshore and WBW transports tend to cancel providing a total transport (−14.6 Sv) in better agreement with those obtained from RAPID (−16.9 Sv). These results are summarized in Table 2.

In contrast to the large changes seen in the upper layer, both CTL and SYN show very similar total transports below 1500 m (Fig. 4, Table 3). While CTL and SYN have roughly the correct amplitude of upper NADW (1100–3000 m) transport (−12.7 Sv and −13.4 Sv respectively compared to −10.7 Sv for RAPID), both simulations have a significantly weaker southward flow of lower NADW (below 3000 m; −1.6 Sv and −1.8 Sv respectively) than found by C07 (−7.8 Sv). Indeed, a weak northward flow is present below 4000 m which is not present in the estimates of C07. Baehr et al. (2009) obtain a similar feature in their model simulation and attribute the difference to the omission of densities along the flank of the mid-Atlantic ridge in the zonal density gradient calculation from C07, leading to errors in their geostrophic flow estimates. An updated transport estimate from the RAPID array (Kanzow et al., 2010) that uses

---

[2]The observations assimilated here are dominated by those provided by Argo. However, as Argo floats tend to remain in waters

---

deeper than 2000 m, few observations were assimilated on the shelf near the Bahamas. In addition, most assimilation methods (including the method used here) down-weight hydrographic data on the shelf, due to the presence of unresolved processes in the observations (so-called "representivity error"), which can cause spurious mixing and numerical noise if the model is constrained too tightly to the data.

[3]This flow is present in both 1° and 1/4° models and is related to a local recirculation of the northward Florida Current transport. An effort was made to correct this circulation by modifying the local bathymetry without success.

densities along the mid-Atlantic ridge confirms this result. However, even compared to the improved estimates of Kanzow et al. (2010; -5.1 Sv), both CTL and SYN show significantly weak transports of the lower NADW. Mean transports for CTL, SYN and RAPID for the various layers are summarized in Table 3.

In summary, the assimilation provides a significant correction to the bias in the subtropical gyre resulting in an intensified offshore transport in better agreement with the RAPID array estimates of C07. However, an erroneous southward surface flow along the east coast of the Bahamas is not corrected through assimilation. These results suggest that to accurately recover the upper layer transports using assimilation, it is important that the assimilation constrains the densities close to boundaries as well, and not just in the deeper waters. This is of particular importance along the western boundary, where model errors may be uncorrelated with those offshore. Indeed, a recent study by Kanzow et al. (2010) has suggested that there is a significant anticorrelation of flows in the western boundary that compensates for offshore transports leading to a significant reduction in the variability in total meridional transport in the upper layer.

4.4 Time series of layer transports

We will now look at the time variability of transports. Following C07, the mid-ocean transports shown here include the western boundary wedge, but exclude the Florida Current. Also, as in Sect. 4.3 (Fig. 4) we use the full model velocity fields to assess transports.

As noted in Sect. 4.3, the assimilation induces a strengthening and overestimation of the southward flow in the thermocline recirculation (Fig. 5a, 0–800 m) due to errors in the WBW, despite an improvement in offshore transports. In addition to the change in amplitude, the variability in SYN is larger on sub-monthly to seasonal time scales and probably reflects aliasing of mesoscale and Rossby wave variability from offshore onto the western boundary densities. The sub-monthly fluctuations in both model runs show little correlation with those from the RAPID array where variability is mostly associated with waves close to the western boundary. On longer timescales, both model runs display a minimum in southward thermocline flow in October in agreement with the RAPID array observations, and longer model simulations show that this minimum is a robust feature of the model seasonal cycle (not shown). In the intermediate waters (Fig. 5b, 800–1000 m), both CTL and SYN have roughly the same amplitude of flow as found by C07, with SYN again showing a slightly larger variability.

The impact of assimilation on the deeper waters is relatively minor. For the upper NADW (Fig. 5c, 1100–3000 m), both simulations have a weak sub-annual variability, which is not improved by the assimilation. The lower NADW transport (Fig. 5d, below 3000 m) also shows a weak sub-annual variability with little influence from assimilation. In addi-
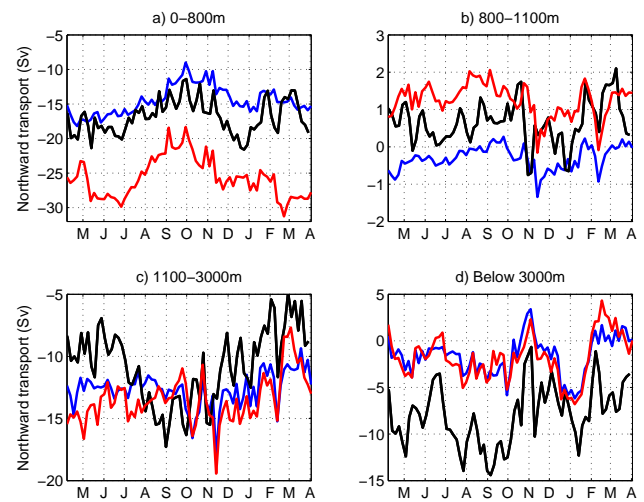
Fig. 5. Time series of northward layer transports for the thermocline (0–800 m) **(a)**, intermediate water (800–1100 m) **(b)**, upper NADW (1100–3000 m) **(c)** and lower NADW (3000–4730 m) **(d)**. Time series are shown for the RAPID array estimates of C07 (black), CTL (blue) and SYN (red). The estimates of C07 have been averaged over the same 5 day periods as the model output to facilitate visual comparison. All values are given in Sverdrups (1 Sv$=10^6$ m^3/s).

tion, the RAPID observations show a strong intensification of southward flow in the spring and fall of 2004, which is only weakly captured by the model simulations. However, both model simulations do show a strong southward pulse in early 2005 in agreement with the RAPID timeseries of C07.

4.5 Time series of AMOC components

We now turn our attention to the impact of data assimilation on the transport timeseries of AMOC components (Florida Current, Ekman and mid-ocean transports) as determined by the RAPID monitoring system (and described in C07). Figure 6 shows the three AMOC components along with the total AMOC (mean values are summarized in Table 4). The "upper mid-ocean" transport includes the full transport from Abaco Island to Morocco integrated down to 1100 m and is equivalent to the sum of transports shown in Fig. 5a and b.

As expected, the Ekman transports are nearly identical between C07 and the model experiments, with small instantaneous differences (1–2 Sv) occurring due to the different wind stress products used (QuikScat and ECMWF analyses respectively). Some additional minor differences are present between experiments due to the dependence of the wind stress formulation on the surface currents.

Due to the erroneous southward WBW transport (Fig. 4b), the southward mid-ocean transport in SYN is too strong compared to RAPID (Fig. 6d) by roughly 8 Sv. The intensification of the mid-ocean transport in SYN over that in CTL is accompanied by an increase in both the mean and variability of the northward flow of the Florida Current (Fig. 6a).
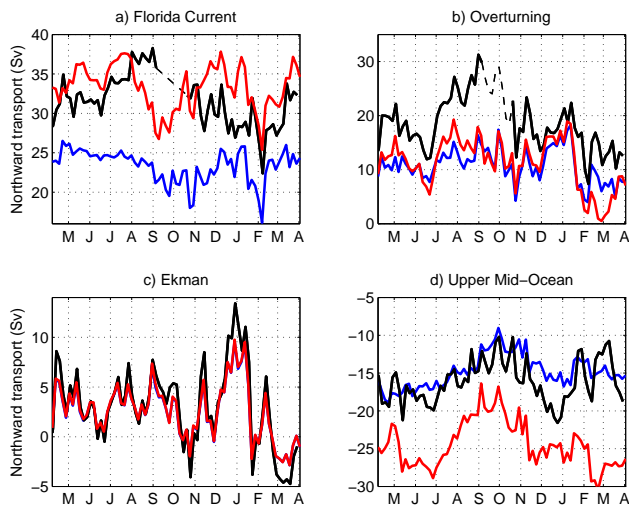
Fig. 6. Time series of Florida Current transport **(a)**, AMOC **(b)**, Ekman transport **(c)** and mid-ocean transport **(d)** for the period April 2004 to April 2005. Time series are shown for the RAPID array estimates of C07 (black), CTL (blue) and SYN (red). The estimates of C07 have been averaged over the same 5 day periods as the model output to facilitate visual comparison. All values are given in Sverdrups (1 Sv=10^6 m^3/s).

Table 4. Annual-mean AMOC and components of the AMOC at 26.5° N (April 2004–March 2005). AMOC components are defined following C07. The RAPID values are quoted from C07.

Transport	Florida Current	Ekman	Mid-ocean	AMOC
CTL	23.3 Sv	2.6 Sv	−14.9 Sv	10.9 Sv
SYN	33.3 Sv	2.7 Sv	−24.4 Sv	11.2 Sv
RAPID (C07)	31.7 Sv	3.0 Sv	−16.1 Sv	18.7 Sv

In particular, significant sub-annual variability of the Florida Current transport is excited by the assimilation. The mean amplitude of the Florida Current transport in SYN (33.3 Sv) is in better agreement with observed cable measurements (31.7 Sv) as compared to CTL (23.3 Sv), although the variations are not correlated.

The large changes in the amplitude and variability of the mid-ocean and Florida Current transports in SYN show a nearly perfect compensation, such that there is remarkably little change to the overturning circulation (Fig. 6b). Indeed, the mean amplitude of the overturning in SYN (11.2 Sv) is only 0.3 Sv larger than that of CTL (10.9 Sv), despite a 10.0 Sv increase in the mean amplitude of the Florida Current transport. Therefore the changes imposed by the assimilation to the upper layer density appear to project almost entirely onto the subtropical gyre circulation, with little influence on the overturning. Moreover, because the assimilation does not adequately constrain the transports in the WBW, sub-monthly variations in the mid-ocean and Florida Current
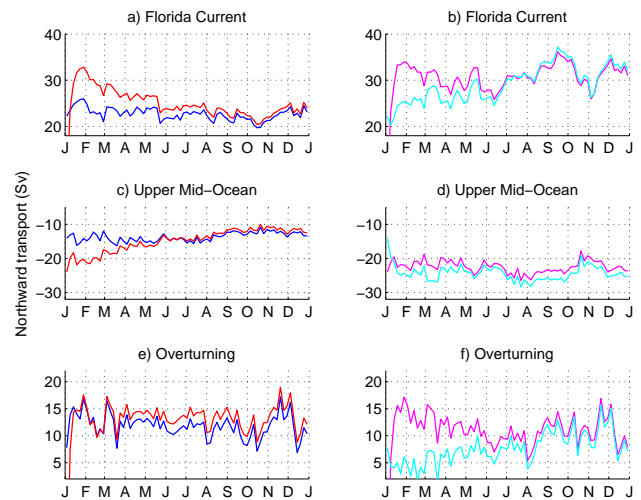
Fig. 7. Time series of Florida Current transport **(a, b)**, upper mid-ocean transport **(c, d)** and AMOC **(d, e)** for the period January 2002 to January 2003. The left column shows timeseries for CTL (blue) and CTL-IC (red) and the right column for SYN (cyan) and SYN-IC (magenta). All values are given in Sverdrups (1 Sv=10^6 m^3/s).

transports are not captured either. In addition, this gyre response to zonal density changes appears to be a robust feature as it is also reproduced in the 1/4° resolution model experiments (see supplementary material, Figs. S3 and S4) as well as in longer simulations of the 1° resolution model (not shown).

5 Sensitivity to initial conditions

The assimilation experiments discussed above have all been initialized from the spun-up control run and thus begin with large water mass errors, which have developed in CTL since the initialization in 1958. Here we seek to examine the timescales on which the AMOC responds to local density perturbations in experiments that begin with more correct density gradients that we then seek to maintain through assimilation. A better knowledge of the timescales of AMOC adjustment will highlight the physical processes involved in the adjustments and shed light on how best to maintain a balanced model circulation.

Two additional simulations are considered: CTL-IC uses no assimilation and is initialized from the WOA climatology in January 2002, and SYN-IC is the same as CTL-IC except with data assimilation. Timeseries of the Florida Current transport, the upper mid-ocean transport and the AMOC for these four simulations are shown in Fig. 7 for the period January 2002–January 2003. After a fast initial spin-up of the circulation in CTL-IC taking only a few days, the AMOC variability (Fig. 7e) is nearly identical to that of CTL but differs by being persistently higher by about 2 Sv

bringing the results closer to those of RAPID. Also CTL-IC initially has a much stronger subtropical gyre circulation, which is reflected in the stronger southward upper mid-ocean transport (Fig. 7c) and northward Florida Current transport (Fig. 7a). Over a period of about 6 months, the zonal density gradients relax until the Florida Current transport and the upper mid-ocean transport both reach values within 1 Sv of the CTL simulation, with the Florida Current transport being 1 Sv stronger and the upper mid-ocean return flow being 1 Sv weaker, providing for the extra 2 Sv of overturning. This adjustment of the gyre circulation is independent of the AMOC and is a further example of the decoupling of the gyre and AMOC components discussed in Sect. 4.5. Figure 8 (left panels) shows the mid-ocean transport breakdown by depth layers. The persistently stronger southward flow of lower NADW below 3000 m and weaker southward flow of upper NADW (1100–3000 m) for CTL-IC are clear. In particular, the stronger lower NADW transport at the end of 2002 in CTL-IC of about 3 Sv is in better agreement with the RAPID mean value (7.8 Sv; Table 3) than CTL (1.6 Sv). Moreover, these differences are still detectable after 3 years (Fig. S6).

A comparison of the transports for SYN and SYN-IC is shown in the right panels of Figs. 7 and 8. Over the first month the temperature and salinity fields for both SYN and SYN-IC undergo significant modification and converge rapidly, resulting in very similar upper mid-ocean transports (Fig. 7d). The resulting transports have a similar strength to the initial transports in CTL-IC, with values considerably high compared to observations (see Table 3). The Florida Current transport in SYN-IC reaches a high value over 30 Sv immediately following initialization as in CTL-IC, but remains high instead of dropping back on a 6 month timescale as in CTL-IC. In constrast, it takes about 6 months for the Florida Current transport in SYN to get above 30 Sv (Fig. 7b). During this period of Florida Current adjustment in SYN, there is a strong southward component to the gyre circulation, and a weak Florida Current transport which together result in a very weak AMOC of about 5 Sv (Fig. 7f). During this adjustment the stronger southward upper mid-ocean flow is compensated by a northward barotropic flow (mostly along the western boundary) which affects the deeper transports seen in Fig. 8d,f. Note that the transports for SYN-IC and CTL-IC for the deep layers below 1100 m have very similar amplitudes over most of the first year because there is little correction to the zonal density gradients in SYN-IC at these depths.

6 Discussion

Clearly, there are still many challenges in constraining the meridional overturning circulation in ocean or climate models. Dunstone and Smith (2010) show that by assimilating full fields of temperature and salinity over the upper 2000 m they are able to reconstruct the AMOC in an idealized frame-
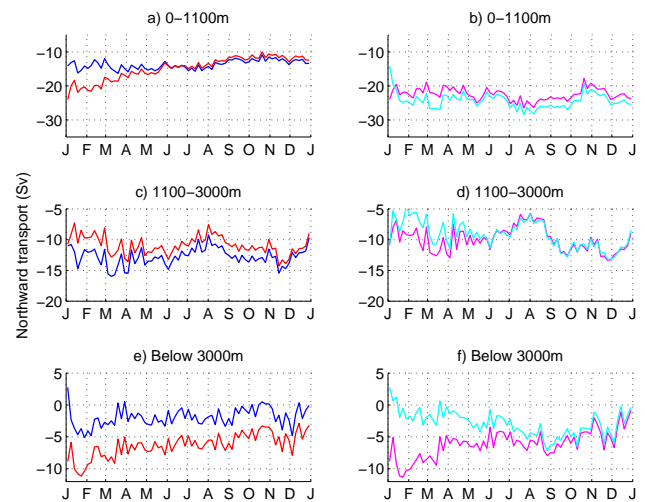
Fig. 8. Time series of layer transports for the upper 1100 m **(a, b)**, upper NADW (1100–3000 m) **(c, d)** and lower NADW (3000–4730 m) **(d, e)** for the period January 2002 to January 2003. The left column shows time series for CTL (blue) and CTL-IC (red), and the right column for SYN (cyan) and SYN-IC (magenta). All values are given in Sverdrups (1 Sv=10^6 m^3/s).

work. In contrast, we find that assimilation of actual upper layer hydrographic data, even with the Argo dataset, is not sufficient to constrain the Atlantic AMOC at 26.5° N. A major reason for this is because the assimilation fails to constrain the deep density gradients below 2000 m and those directly along the western boundary. A consequence of this is that circulation changes resulting from assimilation are reflected in gyre transports rather than AMOC transports. To assess the impact of modifying the deeper water masses, we did perform some preliminary experiments assimilating the RAPID array data itself into the model (not shown). However, when the deep RAPID array observations are assimilated using standard Gaussian covariance scales, large changes in dynamic height can develop around the RAPID moorings resulting in a deterioration of the local circulation. A more careful approach may thus be needed, for example, involving boundary specific covariances associated with lower NADW variability and bias.

One of the key aims for developing an ocean assimilation system that can determine the AMOC is to support climate predictions. The poleward ocean heat transport controlled by the AMOC play a key role in controlling climate in and downstream of the North Atlantic. If the AMOC can be initialized through ocean assimilation this may help predict some aspects of North Atlantic climate variability on timescales out to a few years. The results presented here (in Sect. 5), show that an improved representation of deep water masses in the initial conditions (i.e. CTL vs. CTL-IC) can persist for periods longer than 3 years and result in an improved AMOC at 26.5° N. However, simply correcting the

large-scale upper layer zonal density gradient does not result in a better AMOC. Moreover, when the assimilation disturbs the sensitive balance in the gyre circulation between the mid-ocean and the Florida Current a significant deterioration of the AMOC can occur. Even if a particular gyre intensity in the initial condition is not supported by the model and a bias develops (as found here), as long as the balance between the mid-ocean and the Florida Current transport is maintained, then the AMOC is unaffected. While the particular bias found here may be model dependent, the results do demonstrate a basic requirement that the data assimilation method must maintain a balanced gyre circulation or the AMOC will be impacted negatively. The results here, particularly on the persistence of the better AMOC with improved initial lower NADW distributions, do suggest that AMOC predictions of several years may be possible provided the deeper waters are correctly initialized and a balanced gyre is maintained. This is promising for the development of decadal forecasting capabilities.

These results also suggest that to accurately constrain the modelled AMOC with data assimilation, errors in the deeper water masses should be addressed. This implies that while the RAPID monitoring array at 26.5° N provides valuable information about the state of the overturning and heat transport in the North Atlantic, it may not be the ideal observing system by itself to aid in initializing coupled model AMOC predictions. An additional observing system providing information about the state of dense waters throughout the Atlantic could be of great benefit. For example, this could be achieved through the occasional profiling to 4–5 km depth by a small subset of Argo floats. However, the results presented here do show some evidence of the benefits of assimilation of Argo at higher latitudes on the AMOC at 26.5° N. This result is consistent assertions made by previous studies, for example, Balmaseda et al. (2007) that demonstrate an improvement in the modelled AMOC with data assimilation in a multi-decadal reanalysis. Further work using long reanalyses are required to evaluate the extent to which assimilation can improve dense water formation, and thus improve the AMOC.

Finally, it has been suggested that sequential data assimilation may induce gravity wave noise which could induce spurious mixing that would negatively impact on the model AMOC. Here, we obtain only a small difference in AMOC with assimilation (i.e. between CTL and SYN), despite a radical impact on the gyre circulation. This is evidence that the assimilation is not adversely affecting the water masses through spurious mixing.

7 Conclusions

Here, we have presented a detailed comparison of model simulations with and without sequential data assimilation to the observations and transport estimates from the RAPID mooring array across 26.5° N in the Atlantic. Comparisons of modelled water properties with the observations from the merged RAPID boundary arrays demonstrate the ability of in situ data assimilation to tightly constrain the east-west density gradient between these mooring arrays. However, the presence of an unconstrained "western boundary wedge" between Abaco Island (the Bahamas) and the RAPID mooring site WB2 (16 km offshore) leads to the intensification of an erroneous southwards flow in this region when in situ data are assimilated. The result is an overly intense southward upper mid-ocean transport (0–1100 m) as compared to the estimates derived from the RAPID array (C07). In addition, the sub-seasonal variability of both the mid-ocean and Florida Current transports is not well recovered by the assimilation. This highlights the importance of processes near the western boundary in setting the zonal pressure gradient (and the AMOC), rather than the zonal density gradient as observed close to, but not at, the western boundary.

Correction of upper layer zonal density gradients is found to compensate mostly for a weak subtropical gyre circulation in the free model run (i.e. with no assimilation). The rapid intensification of the zonal density gradient (and southwards thermal wind), leads to a fast barotropic response with a northward flow focused near the western boundary. The northward barotropic flow results in a reduction in southwards transport of the upper and lower NADW and hence a slowing of the AMOC. Gradually, over a period of 6 months the Florida Current transport intensifies in response to the stronger zonal density gradient allowing the northward barotropic circulation to slacken and the AMOC to return to its previous amplitude.

Despite the important changes to the density structure and transports in the upper layer imposed by the assimilation, very little change occurs in the AMOC after the initial 6 month adjustment is made to the gyre amplitude. This shows that assimilation of upper layer density information is absorbed mainly by the gyre circulation with little effect on the AMOC due to the absence of corrections to density gradients below 2000 m (the maximum depth of Argo). An assimilation experiment in a higher resolution eddy-permitting 1/4° resolution model further supports the finding that the primary response to upper layer hydrographic assimilation at 26° N is in the strength of the gyre and not the AMOC. This response was also found to be robust to changes in model bathymetry near the western boundary (not shown), and details of sea surface height and geostrophic velocity balancing increments applied by the assimilation (not shown). However, it should be noted that this response may be dependent on the model and assimilation method employed here.

The sensitivity to initial conditions was explored through use of two additional experiments using a climatological initial condition. These experiments showed that the weak bias in gyre intensity in the control simulation (without data assimilation) develops over the period of about 6 months, but does so independently from the overturning, with no change to AMOC. However, differences in the properties and volume of NADW persisted throughout the 3 year simulations resulting in a difference of several Sverdrups in AMOC intensity. The persistence of these dense water anomalies and their influence on the AMOC is promising for the development of decadal forecasting capabilities. However, the results found here suggest that the deeper waters must be accurately initialized in order to constrain the AMOC. This highlights the need for deep ocean profiling floats which can be used to constrain the circulation and properties of the dense waters present at depth. Further study is required using longer simulations to fully understand the extent to which the deeper waters at 26.5° N are constrained by assimilation at higher latitudes.

Supplementary material related to this article is available online at: http://www.ocean-sci.net/6/761/2010/ os-6-761-2010-supplement.pdf.

References

Adcroft, A., Hill, C., and Marshall, J.: Representation of topography by shaved cells in a height coordinate ocean model, Mon. Weather Rev., 125, 2293–2315, 1997.

Balmaseda, M. A., Smith, G. C., Haines, K., Anderson, D., Palmer, T. N., and Vidard, A.: Historical reconstruction of the Atlantic Meridional Overturning Circulation from the ECMWF operational ocean reanalysis, Geophys. Res. Lett., 34, L23615, doi:10.1029/2007GL031645, 2007.

Baringer, M. O. and Larsen, J. C.: Sixteen years of Florida Current transport at 27° N, Geophys. Res. Lett., 16, 3179–3182, doi:10.1029/2001GL013246, 2001.

Barnier, B., Brodeau, L., Le Sommer, J., and coauthors: Eddy-permitting Ocean Circulation Hindcasts of Past Decades, CLIVAR Exchanges, 12(3), 8–10, 2007.

Barnier, B., Madec, G., Penduff, T., Molines, J.-M., Treguier, A.-M., Le Sommer, J., Beckmann, A., Biastoch, A., Böning, C., Dengg, J., Derval, J., Durand, E., Gulev, S., Remy, E., Talandier, C., Theetten, S., Maltrud, M., McClean, J., and De Cuevas, B.: Impact of partial steps and momentum advection schemes in a global ocean circulation model at eddy-permitting resolution, Ocean Dynam., 56, 6543–6567, doi:10.1007/s10236-006-0082-1, 2008.

Baehr, J., Cunnningham, S., Haak, H., Heimbach, P., Kanzow, T., and Marotzke, J.: Observed and simulated estimates of the meridional overturning circulation at 26.5° N in the Atlantic, Ocean Sci., 5, 575–589, doi:10.5194/os-5-575-2009, 2009.

Blanke, B. and Delecluse, P.: Variability of the Tropical Atlantic Ocean Simulated by a General Circulation Model with Two Different Mixed-Layer Physics, J. Phys. Oceanogr., 23, 1363–1388, 1993.

Bloom, S. C., Tacks, L. L., daSilva, A. M., and Ledvina, D.: Data assimilation using incremental analysis updates, Mon. Weather Rev., 124, 1256–1271, 1996.

Boyer, T. P., Garcia, H. E., Johnson, D. R., Locarnini, R. A., Mishonov, A. V., Pitcher, M. T., Baranova, O. K., and Smolyar, I. V.: World Ocean Database 2005, NOAA Atlas NESDIS 60, edited by: Levitus, S., US Gov. Print. Off., Washington DC, 190 pp., 2006.

Brodeau, L., Barnier, B., Treguier, A.-M., Penduff, T., and Gulev, S.: An ERA40 based atmospheric forcing for global ocean circulation models, submitted to Ocean Model., 31, 88–104, doi:10.1016/j.ocemod.2009.10.005, 2010.

Bryden, H. L., Longworth, H. L., and Cunningham, S. A.: Slowing of the Atlantic Meridional Overturning Circulation at 25° N, Nature, 438, 655–657, 2005.

Collins, M. and Sinha, B.: Predictability of decadal variations in the thermohaline circulation and climate, Geophys. Res. Lett., 30(6), 1306, doi:10.1029/2002GL016504, 2003.

Collins, M., Botzet, M., Carril, A. F., and coauthors: Interannual to decadal climate predictability in the North Atlantic: A multimodel-ensemble study, J. Climate, 19, 1195–1203, 2006.

Conkright, M. E., Locarnini, R. A., Garcia, H. E., O'Brian, T. D., Boyer, T. P., Stephens, C., and Antonov, J. I.: World Ocean Atlas 2001: Objective Analyses, Data Statistics, and Figures, CD-ROM Documentation, National Oceanographic Data Center, Silver Spring, MD, 17 pp., 2002

Cunningham, S. A., Kanzow, T., Rayner, D., Baringer, M. O., Johns, W. E., Marotzke, J., Longworth, H. R., Grant, E. M., Hirschi, J. J.-M., Beal, L. M., Meinen, C. S., and Bryden, H. L.: Temporal Variability of the Atlantic Meridional Overturning circulation at 26.5° N, Science, 317, 935–938, doi:10.1126/science.1141304, 2007.

Dunstone, N. J. and Smith, D. M.: Impact of atmosphere and subsurface ocean data on decadal climate prediction, Geophys. Res. Lett., 37, L02709, doi:10.1029/2009GL041609, 2010.

Fichefet, T. and Maqueda, M. A. M.: Sensitivity of a global sea ice model to the treatment of ice thermodynamics and dynamics, J. Geophys. Res., 102, 12609–12646, 1997.

Gemmell, A., Smith, G. C., Haines, K., and Blower, J.: Ocean model-data analyses with OceanDIVA, J. Operat. Oceanogr.,

2(2), 29–41, 2009.

Gemmell, A., Smith, G. C., Haines, K., and Blower, J.: Evaluation of water masses in ocean synthesis products, CLIVAR Exchanges, 13(4), 7–9, 2008.

Gent, P. R. and McWilliams, J. C.: Isopycnal Mixing in Ocean Circulation Models, J. Phys. Oceanogr., 20, 150–155, 1990.

Goose, H. and Fichefet, T.: Importance of ice-ocean interactions for the global ocean circulation: A model study, J. Geophys. Res., 104(23), 23337–23355, 1999.

Gould, J.: From swallow floats to Argo – The development of neutrally buoyant floats, Deep Sea Res. Pt. I, 52, 529–543, 2005.

Griffies, S. M. and Bryan, K.: Predictability of North Atlantic multidecadal climate variability, Science, 275, 181–184, 1997.

Haines, K., Blower, J., Drecourt, J.-P., Liu, C., Vidard, A., Astin, I., and Zhou, X.: Salinity assimilation using S(T) relationships, Mon. Weather Rev., 134, 759–771, 2006.

Ingleby, B. and Huddleston, M.: Quality control of ocean temperature and salinity profiles—Historical and real-time data, J. Mar. Syst., 65, 158–175, 2007.

Jansen, E., Overpeck, J., Briffa, K. R., Duplessy, J.-C., Joos, F., Masson-Delmotte, V., Olago, D., Otto-Bliesner, B., Peltier, W. R., Rahmstorf, S., Ramesh, R., Raynaud, D., Rind, D., Solomina, O., Villalba, R. ,and Zhang, D.: Palaeoclimate, in: Climate Change 2007: The Physical Science Basis, Contribution of Working Group I to the Fourth Assessment Report of the Intergovernmental Panel on Climate Change, edited by: Solomon, S., Qin, D., Manning, M., Chen, Z., Marquis, M., Averyt, K. B., Tignor, M., and Miller, H. L., Cambridge University Press, Cambridge, UK and New York, NY, USA, 2007.

Juza, M., Penduff, T., Barnier, B., and Brankart, J. M.: Analysis of monthly ARGO sampling errors in the global ocean mixed layer: a DRAKKAR model study, in preparation, 2010.

Kanzow, T., Cunningham, S. A., Rayner, D., Hirschi, J. J.-M., Johns, W. E., Baringer, M. O., Bryden, H. L., Beal, L. M., Meinen, C. S., and Marotzke, J.: Observed flow compensation associated with the MOC at 26.5 N in the Atlantic, Science, 317, 938–941, 2007.

Kanzow, T., Hirschi, J. J-M., Meinen, C., Rayner, D., Cunningham, S. A., Marotzke, J., Johns, W. E., Bryden, H. L., Beal, L. M., and Baringer, M. O.: A prototype system for observing the Atlantic meridional overturning circulation – scientific basis, measurement and risk mitigation strategies, and first results, J. Operat. Oceanogr., 1, 19–28, 2008

Kanzow, T., Johnson, H. L., Marshall, D. P., Cunningham, S. A., Hirschi, J. J.-M., Mujahid, A., Bryden, H. L., and Johns, W. E.: Basin-wide integrated volume transports in an eddy-filled ocean, J. Phys. Oceanogr., 39(12), 3091–3110, doi:10.1175/2009JPO4185.1, 2010.

Kanzow, T., Cunningham, S. A., Johns, W. E., Hirschi, J. J.-M., Marotzke, J., Baringer, M. O., Meinen, C. S., Chidichimo, M. P., Atkinson, C., Beal, L. M., Bryden, H. L., and Collins, J.: Seasonal variability of the Atlantic meridional overturning circulation at 26.5° N, J. Climate, doi:10.1175/2010JCLI3389.1, in press, 2010.

Keenlyside, N. S., Latif, M., Jungclaus, J., Kornblueh, L., and Roeckner, E.: Advancing decadal-scale climate prediction in the North Atlantic sector, Nature, 453, 84–88, doi:10.1038/nature06921, 2008.

Knight, J. R., Allan, R. J., Folland, C. K., Vellinga, M., and Mann, M. E.: A signature of persistent natural thermohaline circulation cycles in observed climate, Geophys. Res. Lett., 32, L20708, doi:10.1029/2005GL024233, 2005.

Köhl, A.: Group 2: Meridional Transports, Oral Presentation at CLIVAR-GSOP Meeting on Ocean Synthesis Evaluation, available at: http://www.clivar.org/organization/gsop/synthesis/synthesis.php, 31 August–1 September, last access: August 2010, 2006.

Large, W. G. and Yeager, S. G.: Diurnal to decadal global forcing for ocean and sea-ice models: The data sets and flux climatologies, Technical Report TN-460+STR, NCAR, 105 pp., 2004.

Madec, G., Delecluse, P., Imbard, M., and Levy, C.: OPA 8.1 general circulation model reference manual, Notes de l'IPSL, University P. et M. Curie, B102 T15-E5, Paris, No. 11, 91 p., 1998.

Madec, G.: NEMO reference manual, ocean dynamics component: NEMO-OPA, Preliminary version, Note du Pole de modélisation, Institut Pierre-Simon Laplace (IPSL), France, No 27 ISSN No 1288-1619, 2008.

Martin, M. J., Hines, A., and Bell, M. J.: Data assimilation in the FOAM operational short-range ocean forecasting system: a description of the scheme and its impact, Q. J. Roy. Meteor. Soc., 133, 981–995, 2007.

Meehl, G. A., Stocker, T. F., Collins, W. D., Friedlingstein, P., Gaye, A. T., Gregory, J. M., Kitoh, A., Knutti, R., Murphy, J. M., Noda, A., Raper, S. C. B., Watterson, I. G., Weaver, A. J., and Zhao, Z.-C.: Global Climate Projections, in: Climate Change 2007: The Physical Science Basis, Contribution of Working Group I to the Fourth Assessment Report of the Intergovernmental Panel on Climate Change, edited by: Solomon, S., Qin, D., Manning, M., Chen, Z., Marquis, M., Averyt, K. B., Tignor, M., and Miller, H. L., Cambridge University Press, Cambridge, UK and New York, NY, USA, 2007.

Penduff, T., Juza, M., Brodeau, L., Smith, G. C., Barnier, B., Molines, J.-M., Treguier, A.-M., and Madec, G.: Impact of global ocean model resolution on sea-level variability with emphasis on interannual time scales, Ocean Sci., 6, 269–284, doi:10.5194/os-6-269-2010, 2010.

Roullet, G. and Madec, G.: Salt conservation, free surface, and varying levels: a new formulation for ocean general circulation models, J. Geophys. Res., 105(23), 23927–23942, 2000.

Smith, D. M., Cusack, S., Colman, A. W., Folland, C. K., Harris, G. R., and Murphy, J. M.: Improved surface temperature prediction for the coming decade from a global climate model, Science, 317, 796–799, 2007.

Smith, G. C. and Haines, K.: Evaluation of the S(T) assimilation method with the Argo dataset, Q. J. Roy. Meteor. Soc., 135, 739–756, 2009.

Troccoli, A. and Haines, K.: Use of the temperature-salinity relation in a data assimilation context, J. Atmos. Ocean. Tech., 16, 2011–2025, 1999.

Vidard, A., Anderson, D. L. T., and Balmaseda, M.: Impact of ocean observation systems on ocean analysis and seasonal forecasts, Mon. Weather Rev., 135, 409–429, doi:10.1175/MWR3310.1, 2007.